



## Research article

# LncRNA-NONMMUT100923.1 regulates mouse embryonic palatal shelf adhesion by sponging miR-200a-3p to modulate medial epithelial cell desmosome junction during palatogenesis

Ming Zhang<sup>b,1</sup>, Jiayan Zhou<sup>b,1</sup>, Yingwen Ji<sup>b</sup>, Shenyou Shu<sup>b,\*</sup>, Mingjun Zhang<sup>b,\*\*</sup>, Yan Liang<sup>a,\*\*\*</sup>

<sup>a</sup> Department of Burn and Plastic Surgery, Affiliated Hospital of Zunyi Medical University, 149 Dalian Road, Zunyi, 563099, Guizhou, China

<sup>b</sup> The Cleft Lip and Palate Treatment Center, Second Affiliated Hospital of Shantou University Medical College, Shantou, 515041, China



## ARTICLE INFO

## Keywords:

Long non-coding RNA  
Desmosome junction  
Cleft palate  
Epithelium

## ABSTRACT

Cleft palate (CP) is a common neonatal craniofacial defect caused by the adhesion and fusion dysfunction of bilateral embryonic palatal shelf structures. Long non-coding RNA (lncRNA) is involved in CP formation with regulatory mechanism unknown. In this study, all-trans retinoic acid (ATRA) was used to induced cleft palate in embryonic mice as model group. The RNA-sequencing was performed to screen differentially expressed genes between the normal and model group on embryonic day 16.5, and the expression of LncRNA-NONMMUT100923.1 and miR-200a-3p, *Cdsn* was confirmed by RT-PCR and western blotting. Colony formation, CCK-8 and EDU assays were performed to measure cell proliferation and apoptosis on mouse embryonic palatal shelf (MEPS) epithelial cells *in vitro*. Fluorescence in situ hybridization (FISH) and dual luciferase activity assays was used to investigate the regulatory effect of LncRNA-NONMMUT100923.1 on miRNA and its target genes. Up-regulation of LncRNA-NONMMUT100923.1 and *Cdsn* while downregulation of miR-200a-3p was found in the model group. The sponging effects of LncRNA-NONMMUT100923 on miR-200a-3p and the target gene relations between *Cdsn* and miR-200a-3p was confirmed. Low expression of miR-200a-3p was related to the increased expressed levels of *Cdsn* and the proliferation of MEPS epithelial cells. Thus, a potential ceRNA regulatory network in which LncRNA-NONMMUT100923.1 regulates *Cdsn* expression by competitively binding to endogenous miR-200a-3p during palatogenesis, which may inhibit MEPS adhesion by preventing the disintegration of the desmosome junction in medial edge epithelium cells. These findings indicate the regulatory role of lncRNA and provides a potential direction for target gene therapy of CP.

## 1. Introduction

In mammals, palatogenesis is a complex process involving the proliferation, migration, and epithelial-mesenchymal transition

\* Corresponding author.

\*\* Corresponding author.

\*\*\* Corresponding author.

E-mail addresses: [syshu@stu.edu.cn](mailto:syshu@stu.edu.cn) (S. Shu), [zhangmingjun030800@163.com](mailto:zhangmingjun030800@163.com) (M. Zhang), [yan.liang524@hotmail.com](mailto:yan.liang524@hotmail.com) (Y. Liang).

<sup>1</sup> These authors contributed equally to this work.

<https://doi.org/10.1016/j.heliyon.2023.e16329>

Received 19 October 2022; Received in revised form 8 May 2023; Accepted 12 May 2023

Available online 19 May 2023

2405-8440/© 2023 The Author(s). Published by Elsevier Ltd. This is an open access article under the CC BY-NC-ND license (<http://creativecommons.org/licenses/by-nc-nd/4.0/>).

(EMT) of palatal midline seam epithelial cells. Adhesion of the bilateral palatal shelves is the key process in palatal fusion [1,2]. This process requires strict cooperation between cells and tissues and temporal and spatial specialization of the extracellular matrix, mesenchymal cells, the desmosome junction, and epithelial cells as prerequisites for palatal fusion [3–5]. During this process, the desmosome junction of medial edge epithelium (MEE) must be disintegrated before EMT [6]. Subsequently, MEE cells of the bilateral palatal shelves can adhere to one another, after which the midline epithelial seam can disappear to ensure mesenchymal continuity and achieve palatal fusion [3,4,7]. Corneodesmosin (*Cdsn*) is a glycoprotein in the hard palate epithelium and a vital component of the desmosome [8]. *Cdsn* regulates cell-cell adhesion and intercellular junctions, which are essential for mammalian development. During palate development, palatal shelves must adhere before the disintegration of the MEE and form a complete palate. This process agrees with the increase in desmosomes in the MEE [6].

Cleft palate (CP) is a common neonatal craniofacial defect caused by the adhesion and fusion dysfunction of bilateral embryonic palatal shelf structures [9,10]. It has a prevalence approaching one in 500–700 births per year [11]. CP can have serious adverse effects on the physical and psychological health and quality of life of children, as well as cause socioeconomic difficulties for both the patients and their families. Most studies have suggested that the etiology of CP mainly involves geographic location, ethnicity, race, economic and social status, genetics, and the environment, as well as their interactions [1,12,13]. However, the specific pathogenesis of CP remains unknown.

Competing endogenous RNA (ceRNA) can control the transcription of other RNAs by competing for shared miRNA response elements (MREs), including long noncoding RNAs (lncRNAs), pseudogenes, and circular RNAs [14]. lncRNA can bind to or share miRNAs through sponging to regulate the expression of target genes at the transcriptional, post-transcriptional, and epigenetic levels [14]. An increasing number of studies have demonstrated that lncRNA can affect CP formation by sponging miRNA [15,16]. For example, Wei et al. reported that the upregulation of ZFAS1 in non-syndromic cleft lip with or without CP mediated by SP1 inhibits cell proliferation and migration and chondrogenic differentiation by inactivating the WNT/ $\beta$ -catenin signaling pathway [17]. miR-200a-3p was reported to be crucial for tumor proliferation and metastasis. Low expression of miR-200a-3p could inhibit the proliferation and metastasis of epithelial ovarian cancer (EOC) [18]. On the other hand, overexpression of miR-200a-3p can inhibit the EMT process of osteosarcoma cells [19]. But its role in the formation of cleft palate by regulating EMT is unclear.

The objective of this study was to explore the molecular mechanisms of lncRNA-NONMMUT100923.1 as a ceRNA during CP formation induced by ATRA. The study revealed a potential ceRNA regulatory network in which NONMMUT100923.1 sponges competitively bind miR-200a-3p to regulate *Cdsn* and provides evidence that ceRNA regulates cleft palate and provides a direction for target gene therapy.

## 2. Methods

### 2.1. Animal model

This study was performed in accordance with and approved by the guidelines of the Animal Experiment Center of Shantou University Medical College (SUMC2019-297). C57BL/6J (8–9 weeks old, approximately 20 g) mice ( $n = 45$ , 15 males, 30 females) were purchased from Vital River Laboratory Animal Technology (Beijing, China). The mice were raised to 9–10 weeks of age. The females and males were mated in a 2:1 ratio from 12:00 p.m. to 8:00 a.m. the next day, which was recorded as embryonic gestation day 0.5 (E0.5). Female mice at E10.5 were weighed and considered pregnant if there was a significant weight increase compared with E0.5. In the model group, pregnant mice were fed with all-*trans*-retinoic acid (70 mg/kg dissolved in vegetable oil) for one time, whereas the normal group was fed the same amount of vegetable oil as previously described [20]. On E16.5, the pregnant mice in both groups were euthanized and the palatal shelves of embryo were collected.

### 2.2. Histological analysis

The embryonic head of the fetus was collected at E16.5 from both groups. The gross morphology of one random embryonic head with the lower jaw and tongue removed in both groups was observed and recorded. Part of the collected samples was fixed with 4% formalin for 6 h and dehydrated in increasing ethanol concentrations (75%, 85%, 95%, 100%). After two washes with xylene, the samples were embedded in paraffin and cut into 3-mm thick slices, which were stained with hematoxylin and eosin for histological examination.

### 2.3. RNA-seq and bioinformatics analysis

RNA was collected from E16.5 embryonic palatal shelves from the model ( $n = 3$ ) and normal ( $n = 3$ ) groups. The RNA-seq data were collected on the Illumina sequencing platform by Shanghai Oebiotech Co. Ltd (Shanghai, China) and were analyzed by the DESeq software [21]. Differentially expressed lncRNA, miRNA, and mRNA between the groups were selected based on the criteria of  $P < 0.05$  and  $|\log_2\text{fold-change (FC)}| > 1$ . Potential ceRNAs were predicted based on the RNA-seq data as follows. 1) miRanda V3.3a was used to predict the miRNA-lncRNA and miRNA-mRNA gene pairs based on the MRE counts. 2) The expression values were subjected to Pearson correlation analysis to predict miRNA-lncRNA pairs, miRNA-mRNA pairs, and lncRNA-mRNA pairs ( $P < 0.05$  and  $\text{COR} > 0.7$ ). 3) The intersection of co-miRNA-lncRNA and co-miRNA-mRNA was obtained from steps 1 and 2. 4) The ceRNA-score was used to predict lncRNA-mRNA pairs (based on the condition of the relatively high density of MREs and that they shared the same miRNA). 5) Co-lncRNA-mRNA pairs were obtained based on the intersection of Pearson correlation analysis and ceRNA score. Finally, the ceRNA

regulatory network was predicted. The EMT-related markers (epithelial markers and mesenchymal markers) between the two groups were also selected based on RNA-seq data.

#### 2.4. Cell culture

Mouse embryonic heads at E16.5 were collected from both groups (normal group (n = 3) vs. model group (n = 3)). The samples were fixed in liquid nitrogen for 5 min and stored at  $-80^{\circ}\text{C}$  for 7 days. The samples were sent to Guangzhou Fitgene Biotechnology Co., Ltd. (Guangdong, China) on dry ice to isolate and culture the palatal shelf epithelial cells. The cells were cultured in Minimum Essential Medium (Hyclone, Logan, UT, USA) containing 10% fetal bovine serum (Hyclone) in a 5%  $\text{CO}_2$  and  $37^{\circ}\text{C}$  incubator (Heracell 150i; Thermo Fisher Scientific, Waltham, MA, USA). Cells from passage 3 were used for subsequent experiments.

#### 2.5. RT-PCR

RNA was collected from mouse embryonic palatal shelves (normal group (n = 3) vs. model group (n = 3)) using Trizol reagent (Invitrogen, Carlsbad, CA, USA) according to the instructions of a Primescript II 1st Strand cDNA Synthesis Kit (Takara Bio, Shiga, Japan). cDNA was synthesized by reverse transcription using fluorescence-quantified PCR (LC480II; Roche, Basel, Switzerland). The thermal cycling program was as follows:  $94^{\circ}\text{C}$  for 3–4 min,  $94^{\circ}\text{C}$  for 39 s,  $60^{\circ}\text{C}$  for 30 s, and  $72^{\circ}\text{C}$  for 30 s, and  $72^{\circ}\text{C}$  for 10 min, after which the sample was maintained at  $16^{\circ}\text{C}$ . The fluorescence signal was collected after the PCR cycles. The primers used to amplify NONMMUT100923.1/miR-200a-3p/*Cdsn* are listed in Table 1.

#### 2.6. Cell transfection

The mouse embryonic palatal shelf (MEPS) epithelial cells from normal group (n = 3) at passage 3 were used for cell transfection. Briefly, four groups, miR-200a-3p, miR-200a-3p inhibition, Negative control (NC), and NC inhibitor, were prepared (Guangzhou Ruibo Biotechnology Co., Ltd., Guangzhou, China). Each sample (1.25  $\mu\text{L}$ ) and 1  $\mu\text{L}$  of Lipofectamine RNAiMAX (Invitrogen) transfection reagent were added to 100  $\mu\text{L}$  of Opti-MEM (Invitrogen) and mixed well for 20 min. The cells were incubated for 4 h, after which the mixture was replaced with a cell growth medium. Gene expression of *Cdsn*, analyzed as described above, and protein expression of *Cdsn*, performed as described below, in transfected cells were investigated after 24 and 36 h, respectively.

#### 2.7. Western blotting

Total protein from transfected cells from the normal group (n = 3) was collected using RIPA protein extraction reagent (Merck KGaA, Darmstadt, Germany), and the protein concentration was determined using a spectrometer (Spectrum, Shanghai, China). Sodium dodecyl sulfate-polyacrylamide gel electrophoresis loading buffer was added to the protein samples, and the proteins were separated using electrophoresis (Power PAC 200, Bio-Rad, Hercules, CA, USA). After transferring the proteins to a polyvinylidene fluoride membrane, the membrane was washed with a western washing solution for 1–2 min. According to the manufacturer's instructions, proteins in the membrane region were probed with a primary antibody (CDSN rabbit pAb, A14602; Abclonal, Wuhan, China) and anti-GAPDH overnight. The membrane was incubated with a secondary antibody (horseradish peroxidase goat anti-rabbit) at approximately  $27^{\circ}\text{C}$  for 1 h. Protein expression was quantified using Quantity One (Bio-Rad).

#### 2.8. Dual luciferase assay

HEK293T cells (Procell, Wuhan, China) were used for the dual luciferase assay. Wild-type and mutant plasmids were constructed and named psiCHECK2.0-NONMMUT100923.1, psiCHECK2.0-mut-NONMMUT100923.1, psiCHECK2.0-*Cdsn*, and psiCHECK2.0-mut-*Cdsn* (n = 3) (Sangon Bioengineering Co., Ltd., Shanghai, China). Each plasmid was co-transfected into HEK293T cells together with miR-200a-3p mimic, blank, and mimic NC. Luciferase activity was detected using a Dual-Luciferase Reporter Assay System (116680119; Invitrogen). Firefly luciferase (F) and *Renilla* luciferase (R) activities were detected using a manual dual fluorescence detector (GloMax bioluminescence detector, Promega), and the activity multiple was calculated.

**Table 1**  
Primer sequences used in RT-PCR.

Gene	Primer (5'→3')
miR-200a-3p	Forward primer TAACACTGTCTGGTAACGATGT
<i>Cdsn</i>	Forward primer TGGCTCTGCCAACAGTTA Reverse primer GATAGGGTTGCTCTGGTGA
NONMMUT100923.1	Forward primer CTACAGGGAGCCACGTAT Reverse primer TGCTCTGAGACTAGGCAAC

## 2.9. FISH

FISH was conducted to detect the localization of NONMMUT100923.1 and miR-200a-3p in MEPS epithelial cells from the normal group ( $n = 3$ ). Briefly, tissue slides (3-mm thick) of the embryonic head were lysed and incubated with Triton X-100 (Gibco, Grand Island, NY, USA) for 37 °C 20 min. The slides were hybridized with the denatured probe overnight at 27 °C. After overnight incubation, 3% bovine serum albumin blocking solution was added and incubated with the slides for 60 min, after which DAPI was added for 5 min. Anti-fluorescence stain was added to the slides, and staining was observed under a laser scanning co-aggregation microscope (TCS SP2 AOBS; Leica, Wetzlar, Germany).

## 2.10. CCK-8 assay

The transfected cells from the normal group ( $n = 3$ ) were used for the CCK-8 assay. Each group of cells was seeded into 96-well plates (Wuxi NEST Biotechnology Co., Ltd, Jiangsu, China) at  $1 \times 10^4$  cells per 100  $\mu$ L of culture medium per well. After 0, 24, 48, and 72 h of culture, the CCK-8 (Biyuntian, Shanghai, China) solution was added (10  $\mu$ L per 100  $\mu$ L culture medium). The mixture was cultured for an additional 4 h, and the OD<sub>450</sub> was measured using a microplate reader (Thermo Fisher Scientific).

## 2.11. Colony formation assay

The transfected cells from the normal group ( $n = 3$ ) were used for a colony formation assay. Each group of cells was seeded into 96-well plates (200 cells per 300  $\mu$ L of culture medium per well). After culture for 7 days, the medium was aspirated, and 200  $\mu$ L of crystal violet was added to each well. After 20 min of incubation, each well was washed with tap water. Images of the colonies were acquired, and the colonies were counted by EliSpot Reader (AID, Germany).

## 2.12. EdU staining

The transfected cells from the normal group ( $n = 3$ ) were used for EdU staining (C10314; Guangzhou Ruibo Biotechnology). Each group of cells was incubated with 100  $\mu$ L of EdU medium for 2 h. The transfected cells were fixed in 4% paraformaldehyde in PBS (100  $\mu$ L per well) for 10–15 min. The cells were incubated with glycine (2 mg/mL) for 10 min, followed by 100  $\mu$ L of penetrating agent (0.5% Triton X-100 in PBS). Apollo staining solution ( $1 \times$ , 100  $\mu$ L) was added to each well for 30 min. Finally, 100  $\mu$ L of  $1 \times$  Hoechst 33342 solution was added to each well for another 30 min. Images were acquired using an inverted microscope (DMI6000B; Leica).

## 2.13. Statistical analysis

SPSS (version 26SPSS, Inc., Chicago, IL, USA) was used for statistical analysis. All experimental data are represented as the mean  $\pm$  stand deviation. Univariate analysis of variance was used for comparison among groups. miRanda V3.3a and Pearson correlation coefficient were used to screen for ceRNAs. Three independent samples were evaluated in all normal and model groups. Each group was repeated three or more times. Significance was considered when  $P < 0.05$ .

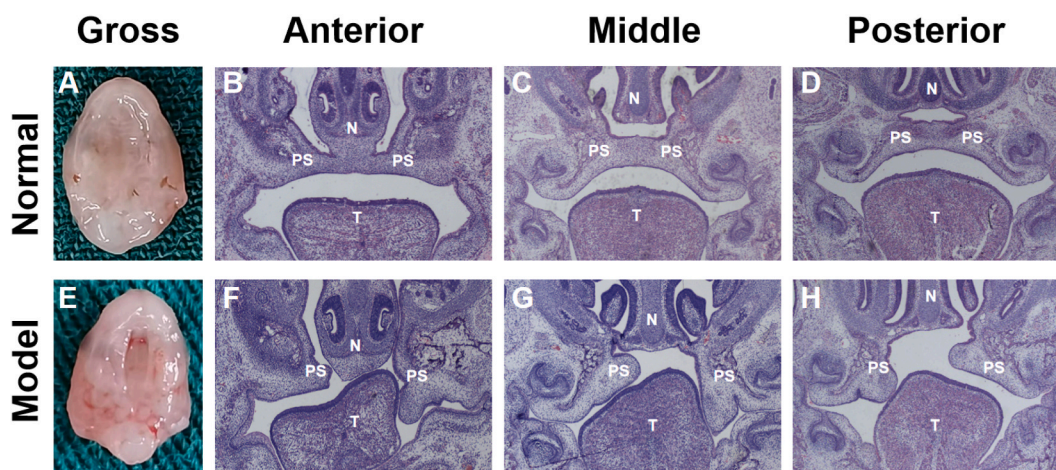


**Fig. 1.** The histological analysis of E16.5 embryonic palatal shelves tissues. Morphological images of the E16.5 embryonic palatal shelves tissues in normal and model groups. (A, E) Gross morphology; (B, C, D, F, G, H) HE staining ( $4 \times 0.1$ ). PS: palatal shelf; T: tongue; N: nose.

### 3. Results

#### 3.1. Morphological of embryonic palate shelves

In terms of gross morphology, the palatal shelves were adhered and fused in the normal group (Fig. 1A), whereas a gap was observed between the palatal shelves in the model group (Fig. 1D). In hematoxylin and eosin staining, the anterior, middle, and posterior views were depicted. Consistent with the gross morphology observations, all palatal shelves were fused in the normal group, forming a complete palatal shelf that separated the oral and nasal cavities. In the model group, one palatal shelf in the anterior (Fig. 1E) and middle (Fig. 1B) views grew vertically along the tongue; neither palatal shelf was evaluated in the posterior view (Fig. 1C). Additionally, tongue descent was delayed according to all three views (Fig. 1F–H). These results demonstrated that the cleft palate model of mouse fetus can be successfully established using the all-*trans*-retinoic acid (70 mg/kg) in this study.

#### 3.2. Overview of RNA expression profiles

To predict the molecular mechanisms of ceRNA, high-throughput sequencing analysis was performed in E16.5 embryonic palatal shelf tissues in the normal and model groups. We identified 770 lncRNAs (Fig. 2A), 88 miRNAs (Figs. 2B), and 1358 mRNAs (Fig. 2C) as differentially expressed between the groups, as depicted in hotspot maps. A volcano map was also plotted to depict the differentially expressed genes ( $P < 0.05$  and  $|\log_2FC| > 1$ ) (Fig. 2D and F).

1) According to the sequencing results, 15393 lncRNA- and 33335 mRNA-miRNA pairs were obtained based on the MRE counts using miRanda V3.3a (Fig. 3A and D). 2) The Pearson correlation coefficient ( $P < 0.05$  and  $COR > 0.7$ ) was used to select related target genes of the differentially expressed miRNAs. We selected 3481 miRNA-lncRNA pairs and 6550 miRNA-mRNA pairs (Fig. 3B and E). 3) The intersection of the 1163 co-lncRNA- and 2768 co-mRNA-miRNAs was obtained from these steps (Fig. 3C and F). 4) The ceRNA score identified 283 pairs of lncRNA-mRNA (Fig. 3G). 5) The Pearson correlation coefficient identified 74730 pairs of lncRNA-mRNA (Fig. 3H). 6) 245 Co-lncRNA-mRNA pairs were also obtained from the overlap of the two lncRNA-mRNA groups (Fig. 3I). RNA-seq data suggested that the expression of NONMMUT100923.1 ( $P = 0.0007$ ;  $\log_2FC = 5.95$ ) and *Cdsn* ( $P = 0.0003$ ;  $\log_2FC = 3.37$ ) was

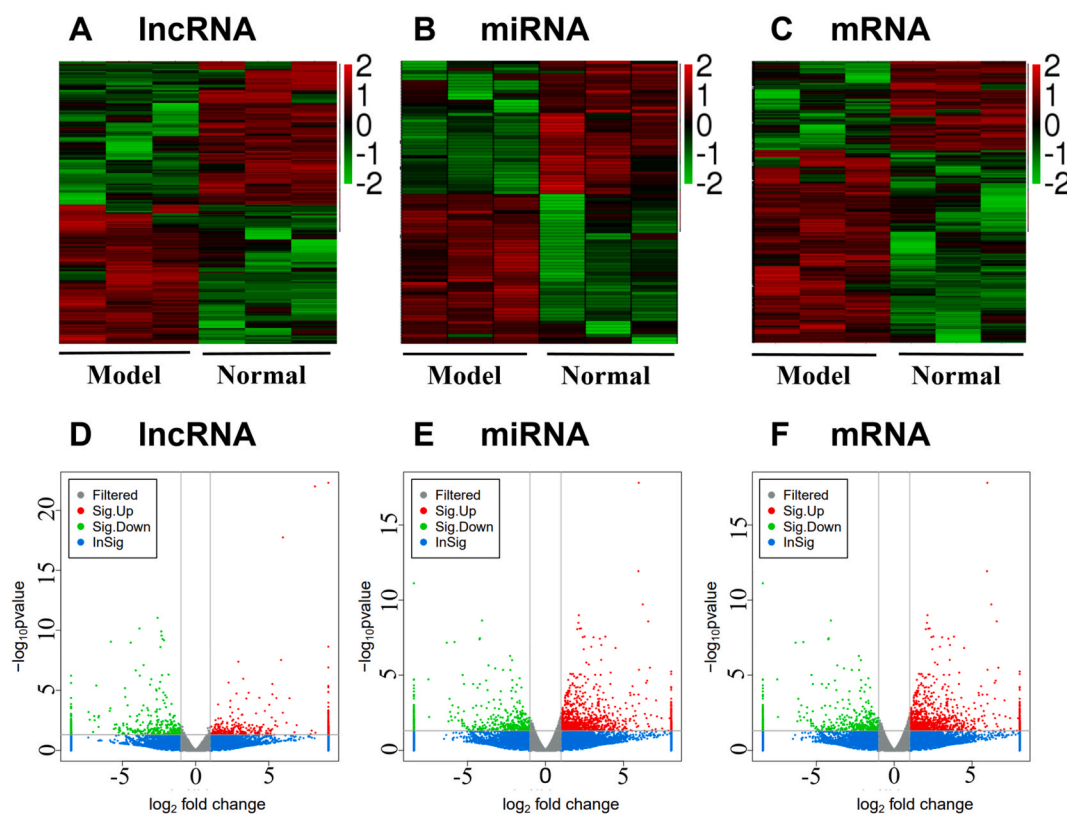


**Fig. 2.** The RNA-seq data analysis. The RNA-seq data were analyzed between the normal and model groups. The hot spot maps of (A) lncRNA, (B) miRNA, and (C) mRNA were showed by the differential expressed gene hierarchical clustering (red colour indicates high expressed genes and green colour indicates low expressed genes; (D, E, F) The volcano maps were showed by the expression level for each gene. The x-axis indicates the  $\log_2FC$ , and the y-axis indicates the  $\log_{10}(p\text{-value})$ . The red dots indicate up-regulated genes and the green dots indicate down-regulated genes, Grey and blue points indicat meaningless. Criteria:  $P < 0.05$  and  $|\log_2FC| > 1$ .

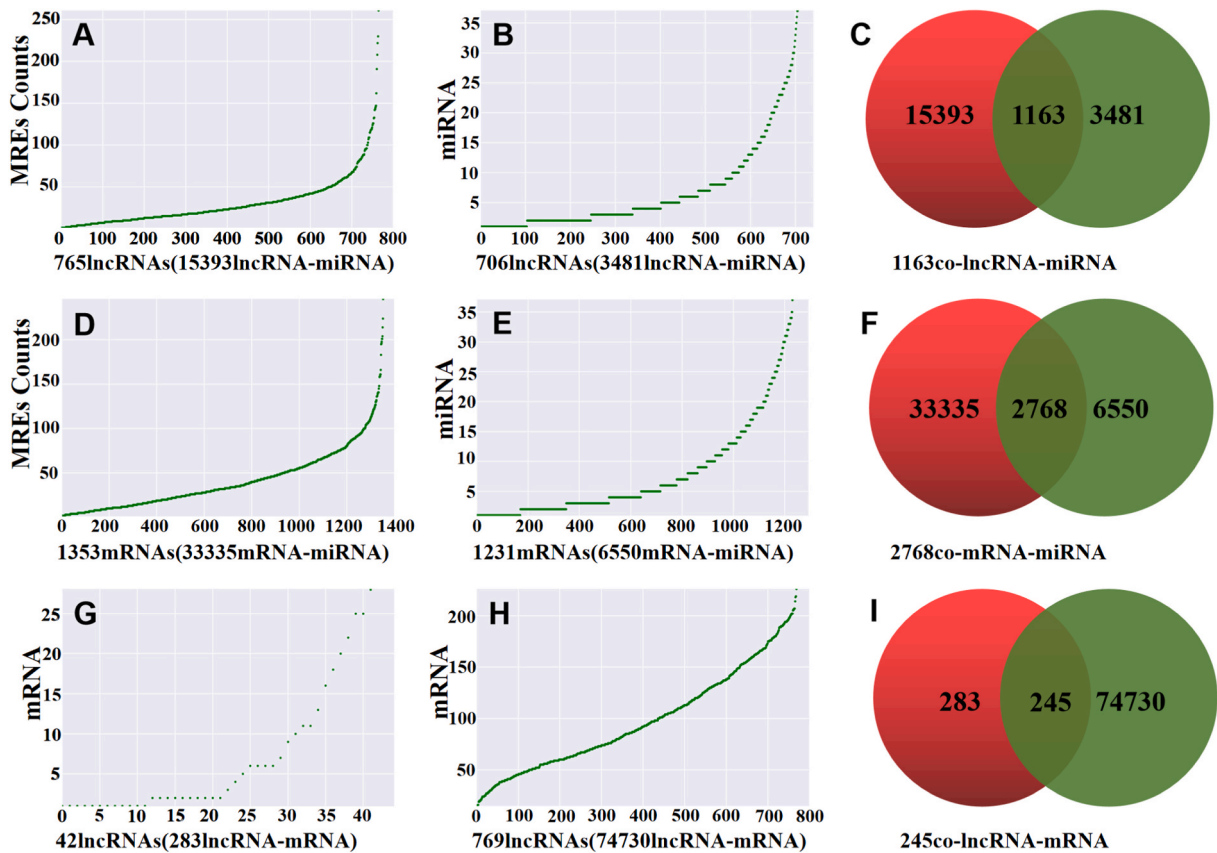


**Fig. 3.** The differential expressed gene analysis. The differential expressed gene were used to predict the potential regulatory mechanics of ceRNA. (A, D) The predicted MREs by miRanda V3.3a software were used to predict the pairs of lncRNA- and mRNA-miRNA; (B, E, H) The Pearson correlation coefficient was used to predict the pairs of lncRNA-miRNA, mRNA-miRNA, and lncRNA-mRNA ( $P < 0.05$  and  $COR > 0.7$ ); (G) The ceRNA score were used to predict the pairs of lncRNA-mRNA; (C, F, I) The intersection of lncRNA-miRNA, mRNA-miRNA, and lncRNA-mRNA.

upregulated in the model group compared with that in the normal group. In contrast, the expression of the miR-200a-3p ( $P = 0.0005$ ;  $\log_2FC = -1.25$ ) was downregulated. Interestingly, *Cdsn* was predicted to be a target gene of miR-200a-3p. Therefore, there may be a possible association among these results that the upregulation of NONMMUT100923.1 sponged miR-200a-3p and led to the down-regulation of miR-200a-3p. Thus, *Cdsn*, the target gene of miR-200a-3p, was upregulated.

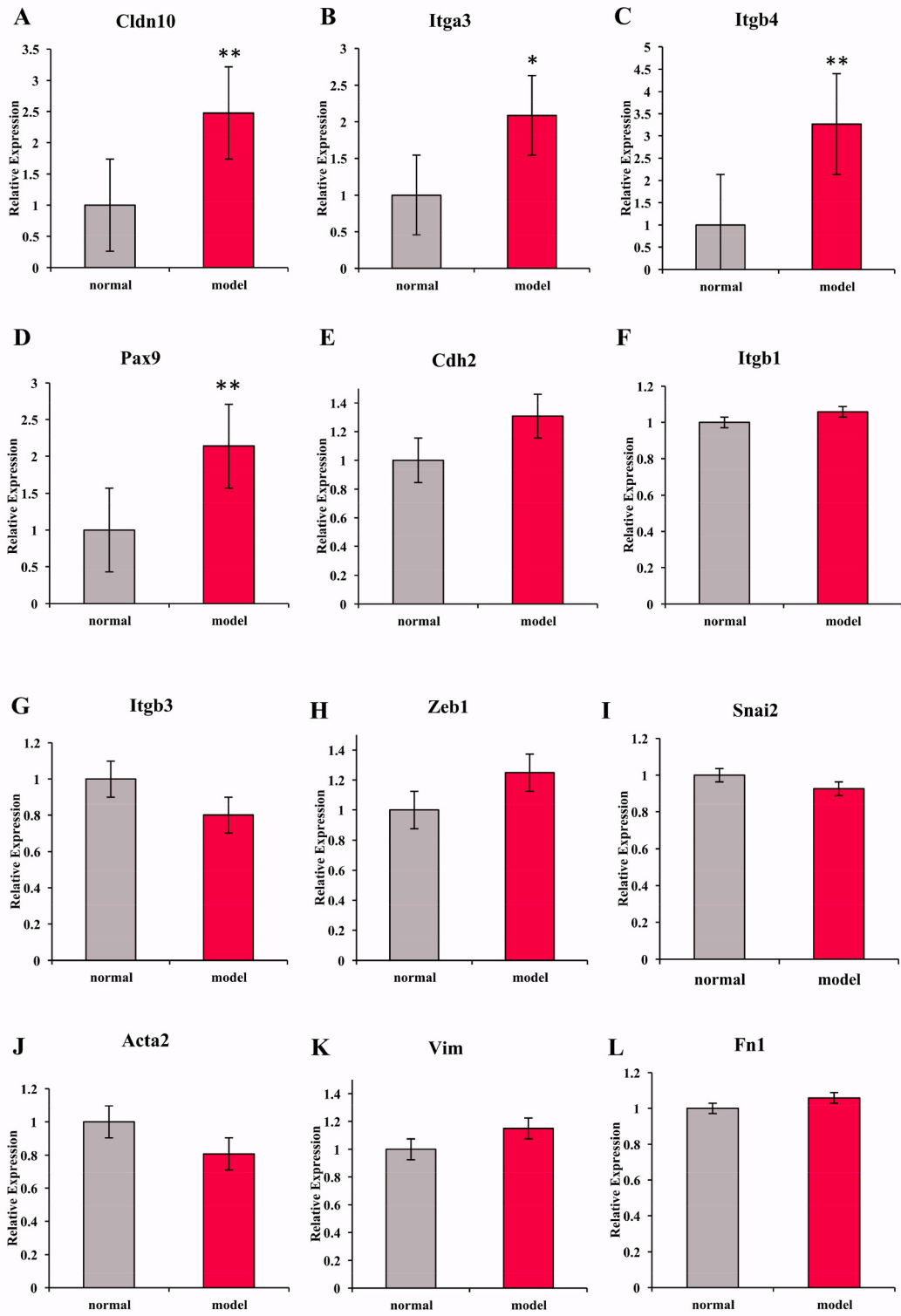
According to the RNA-seq data, the expression levels of represented epithelial markers *Cldn10* ( $P = 0.006$ ,  $FC = 2.477$ ), *Itga3* ( $P = 0.018$ ,  $FC = 2.086$ ), *Itgb4* ( $P = 0.002$ ,  $FC = 3.265$ ) and *Pax9* ( $P = 0.002$ ,  $FC = 2.138$ ) were significantly upregulated between the two groups (Fig. 4A-D, Table 2). However, the expression levels of represented mesenchymal markers, *Vim*, *Fn1*, *Cdh2*, *Itgb1*, *Itgb3*, *Acta2*, *Snai2* and *Zeb1* remained similar between the two groups (Fig. 4E-L, Table 2). These results may indicate that the epithelial cells consistently maintain their phenotype and EMT was not triggered in this mouse model with cleft palate.

### 3.3. RT-PCR validation of ceRNA expression

RT-PCR was used to verify the relative gene expression levels of NONMMUT100923.1, miR-200a-3p, and *Cdsn* in palatal shelf tissues in both groups. In the model group, the expression level of NONMMUT100923.1 was significantly higher than that in the normal group ( $P < 0.01$ : model vs. normal group) (Fig. 5A). In contrast, the expression level of miR-200a-3p was significantly lower in the model group ( $P < 0.01$ : model vs. normal group) (Fig. 5B). The gene expression level of *Cdsn* followed the same trend as NONMMUT100923.1 and was significantly upregulated in the model group ( $P < 0.01$ : model vs. normal group) (Fig. 5C). These results support the potential regulatory relationship mentioned earlier.

### 3.4. Potential regulatory relationship between lncRNA-NONMMUT100923.1 and *Cdsn*

To verify the sponge relationship between NONMMUT100923.1 and miR-200a-3p and potential target relationship between *Cdsn* and miR-200a-3p, a dual fluorescence reporter assay was performed using HEK293T cells. The specific binding sites between NONMMUT100923.1 and miR-200a-3p and *Cdsn* and miR-200a-3p predicted by miRanda are demonstrated in Fig. 6A and B.



(caption on next page)

**Fig. 4.** EMT-related gene analysis. The represented epithelial and mesenchymal markers related to the EMT process were selected based on the mRNA data. Epithelial markers: (A). *Cldn10* (\*\* $P < 0.01$  normal vs. model group); (B). *Itga3* (\* $P < 0.05$  normal vs. model group); (C). *Itgb4* (\*\* $P < 0.01$  normal vs. model group); (D). *Pax9* (\*\* $P < 0.01$  normal vs. model group). Mesenchymal markers: (E–L) nonsense in normal vs. model group. Data are presented as mean  $\pm$  SD from 3 independent samples.

**Table 2**

The expression levels of epithelial markers and mesenchymal markers.

ID	Gene	foldChange	log <sub>2</sub> FC	P-value
ENSMUST00000100314	<i>Cldn10</i>	2.477602526	1.308944759	0.006823126
ENSMUST00000169928	<i>Itgb4</i>	3.26573264	1.707406685	0.001962722
ENSMUST00000001538	<i>Pax9</i>	2.138225423	1.096413957	0.001853726
ENSMUST00000107739	<i>Itga3</i>	2.086808394	1.061298142	0.018144764
ENSMUST00000028062	<i>Vim</i>	1.149427466	0.200915429	0.558206511
ENSMUST00000186129	<i>Fn1</i>	1.058893277	0.082557192	0.919110923
ENSMUST00000115850	<i>Cdh2</i>	1.307713472	0.387046472	0.351367208
ENSMUST00000090006	<i>Itgb1</i>	1.058024805	0.081373451	0.818753497
ENSMUST00000021028	<i>Itgb3</i>	0.800699674	-0.320666876	0.375125188
ENSMUST00000039631	<i>Acta2</i>	0.807454654	-0.308546854	0.560168684
ENSMUST00000023356	<i>Snai2</i>	0.926615674	-0.109957009	0.782323083
ENSMUST00000025081	<i>Zeb1</i>	1.249088008	0.32087513	0.35241539

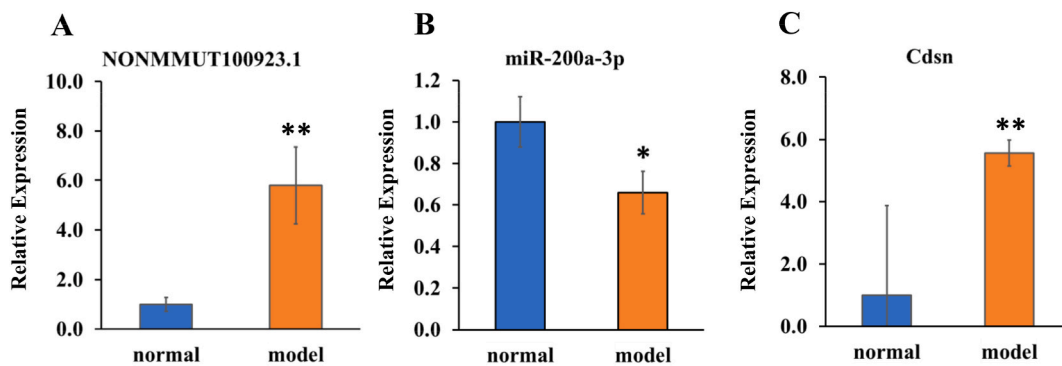


**Fig. 5.** The RT-RCR analysis. The RT-RCR assay was used to verify the relative gene expression levels of NONMMUT100923.1/miR-200a-3p/*Cdsn* between the normal and model groups. (A) The expression levels of NONMMUT100923.1 between the normal and model groups (\*\* $P < 0.01$ ); (B) The expression levels of miR-200a-3p between the normal and model groups (\* $P < 0.05$ ); (C) The expression levels of *Cdsn* between the normal and model groups (\*\* $P < 0.01$ ). Data are presented as mean  $\pm$  SD from 3 independent samples.

NONMMUT100923.1 was significantly decreased in the miR-200a-3p, NC, and blank groups (\*\* $P < 0.01$ : miR-200a-3p vs. blank group and miR-200a-3p vs. NC group in wild-type group), with no significant difference among the three groups (Fig. 6C). Similarly, *Cdsn* fluorescence activity was significantly decreased in the miR-200a-3p, NC, and blank groups (\* $P < 0.05$ : miR-200a-3p vs. blank group in wild type group; \*\* $P < 0.01$ : miR-200a-3p vs. NC group in wild type group); no significant differences were observed among the three groups (Fig. 6D). These results indicated the potential regulatory mechanism between NONMMUT100923.1 and miR-200a-3p, and *Cdsn* and miR-200a-3p.

### 3.5. *LncRNA-NONMMUT100923.1* and miR-200a-3p subcellular localization in embryonic palatal shelf tissues

To confirm the sponge effects between NONMMUT100923.1 and miR-200a-3p, FISH was performed to detect their subcellular locations in the MEPS epithelial cells in the normal group. Both NONMMUT100923.1 (Fig. 7A, red fluorescence), miR-200a-3p (Fig. 7B, green fluorescence) and nucleus (Fig. 7C, blue fluorescence) were expressed in the MEPS epithelial cells. Both were also expressed in the cytoplasm, as indicated by the white arrows in Fig. 7D and E. Some red fluorescence overlapped with the green fluorescence, as indicated by the white arrow in (Fig. 7F). The percentage of cells co-expressing both was  $0.15 \pm 0.03$  (mean  $\pm$  SD). These results suggest that NONMMUT100923.1 and miRNA-200a-3p sponged each other in the palatal shelf tissues, which is consistent with the dual fluorescence reporter results described earlier.

### 3.6. Expression of miR-200a-3p caused *Cdsn* to inhibit MPES epithelial cell proliferation, migration, and EMT

To confirm the target relationship between *Cdsn* and miR-200a-3p, MEPS epithelial cells were transfected with NC mimics, NC

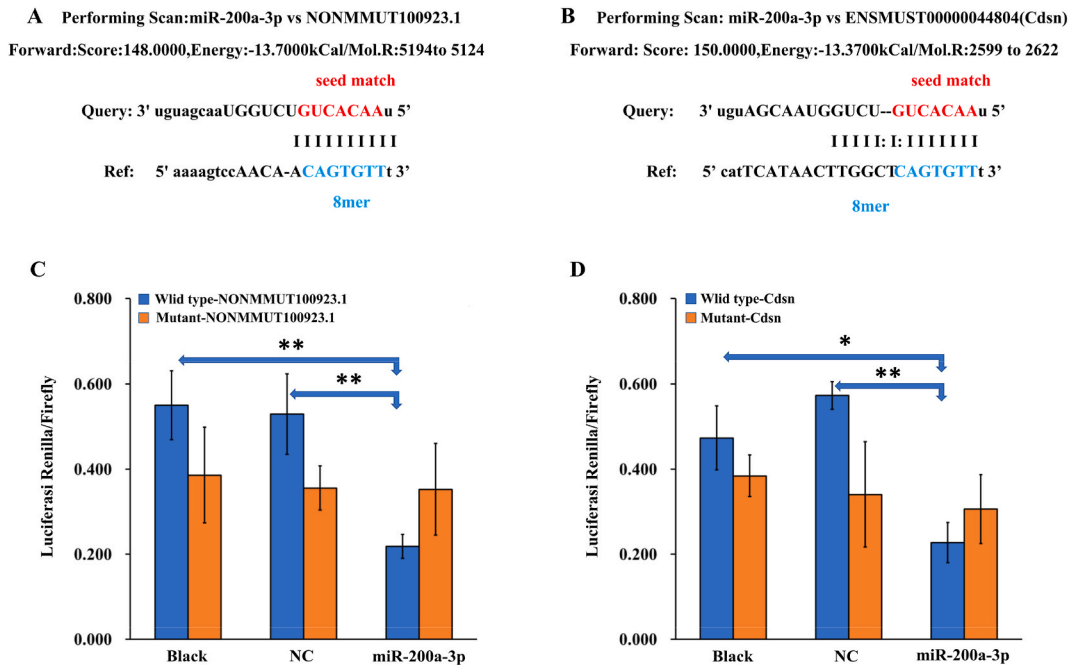


**Fig. 6.** The dual luciferase assay analysis. The dual luciferase assay was used to verify the interaction relationships among miR-200a-3p, NONMMUT100923, and *Cdsn*. (A)The specific binding sites of NONMMUT100923.1 vs. miR-200a-3p; (B)The specific binding sites of *Cdsn* vs. miR-200a-3p; (C) The intensity of luciferase activity after wild-type NONMMUT100923.1 and mutant-NONMMUT100923.1 were co-transfected into HEK293T cells respectively with miR-200a-3p mimic, blank and NC together (\*\* $P < 0.01$ : miR-200a-3p vs. blank group and miR-200a-3p vs. NC group in wild-type group); (D)The intensity of luciferase activity after wild-type *Cdsn* and mutant-*Cdsn* were co-transfected into HEK293T cells respectively with miR-200a-3p, blank and NC together (\* $P < 0.05$ : miR-200a-3p vs. blank group in wild type group; \*\* $P < 0.01$ miR-200a-3p vs. NC group in wild type group). Data are presented as mean  $\pm$  SD from 3 independent samples.

inhibitor, miR-200a-3p, and miR-200a-3p inhibitor. After 24 h, western blotting and RT-PCR were performed to detect the expression levels of *Cdsn*. The RT-PCR results indicated that the relative expression levels of *Cdsn* were significantly downregulated in MEPS epithelial cells transfected with miR-200a-3p compared with those transfected with the NC mimics. In contrast, the *Cdsn* expression level was significantly upregulated in the miR-200a-3p inhibitor group (\*\* $P < 0.001$ : miR-200a-3p vs. NC mimics and miR-200a-3p inhibitor vs. NC mimics) (Fig. 8A). The western blotting results revealed a similar trend for *Cdsn* expression (\*\* $P < 0.001$ : miR-200a-3p vs. NC mimics and miR-200a-3p inhibitor vs. NC mimics) (Fig. 8B and C). To investigate the regulatory effects of miR-200a-3p on MEPS epithelial cells *in vitro*, CCK-8, colony-forming, and EdU assays used applied. In the CCK-8 assay, the proliferation rates of cells transfected with miR-200a-3p were significantly lower than those in the NC mimic group and significantly higher in the miR-200a-3p inhibitor group than in the NC mimic group on day 1, days 2 and 3 (\*\* $P < 0.001$ : miR-200a-3p vs. NC mimics and miR-200a-3p inhibitor vs. NC mimics) (Fig. 8D). In the colony-forming assay, the number of colonies was significantly lower in the miR-200a-3p group and significantly higher in the miR-200a-3p inhibitor group than in the NC mimic group after 7 days of culture (\*\* $P < 0.01$ : miR-200a-3p vs. NC mimics and miR-200a-3p inhibitor vs. NC mimics) (Fig. 8E and F). In the Edu assay, the proliferation ability of cells transfected with miR-200a-3p was similar to that observed in the CCK-8 and colony-forming assays (In 200 $\times$ , \*\* $P < 0.01$ : miR-200a-3p vs. NC mimics; \*\*\* $P < 0.001$ : miR-200a-3p inhibitor vs. NC mimics. In 400 $\times$ , \* $P < 0.05$ : miR-200a-3p vs. NC mimics and miR-200a-3p inhibitor vs. NC mimics) (Fig. 8G and H). In summary, the miR-200a-3p inhibitor promoted the proliferation, migration, and survival of MEPS epithelial cells and reduced apoptosis. Thus, the downregulation of miR-200a-3p resulted in the upregulation of *Cdsn* to maintain the phenotype of epithelial cells and desmosome junction. These effects may inhibit EMT and lead to CP formation.

#### 4. Discussion

Cleft palate is a common congenital maxillofacial disease [22]. Its pathogenesis is complex and remains unknown [9,23]. The disease causes great mental and financial stress to the children and their families [24]. At present, there is limited methods for prenatal prevention and the outcome of surgical treatment is not satisfied [25,26]. Studies have shown that lncRNA is widely involved in cell differentiation, metabolism, and proliferation, and closely related to a variety of diseases [19,27–29]. More importantly, increasing evidence has shown that the lncRNA can regulate maxillofacial diseases, including cleft palate. For example, lncRNAUSP17L6P has been shown to bind to miR-449c-5p and regulate its target genes in patients with non-syndromic cleft lip with or without cleft palate [30]. lncRNA Meg3 was reported to inhibit the proliferation of mouse embryonic palate mesenchymal cells by interacting with Smad2 protein [16] and lncRNA H19 can mediated cleft palate formation in mouse by targeting insulin-like growth factor 2 [31]. In this study,

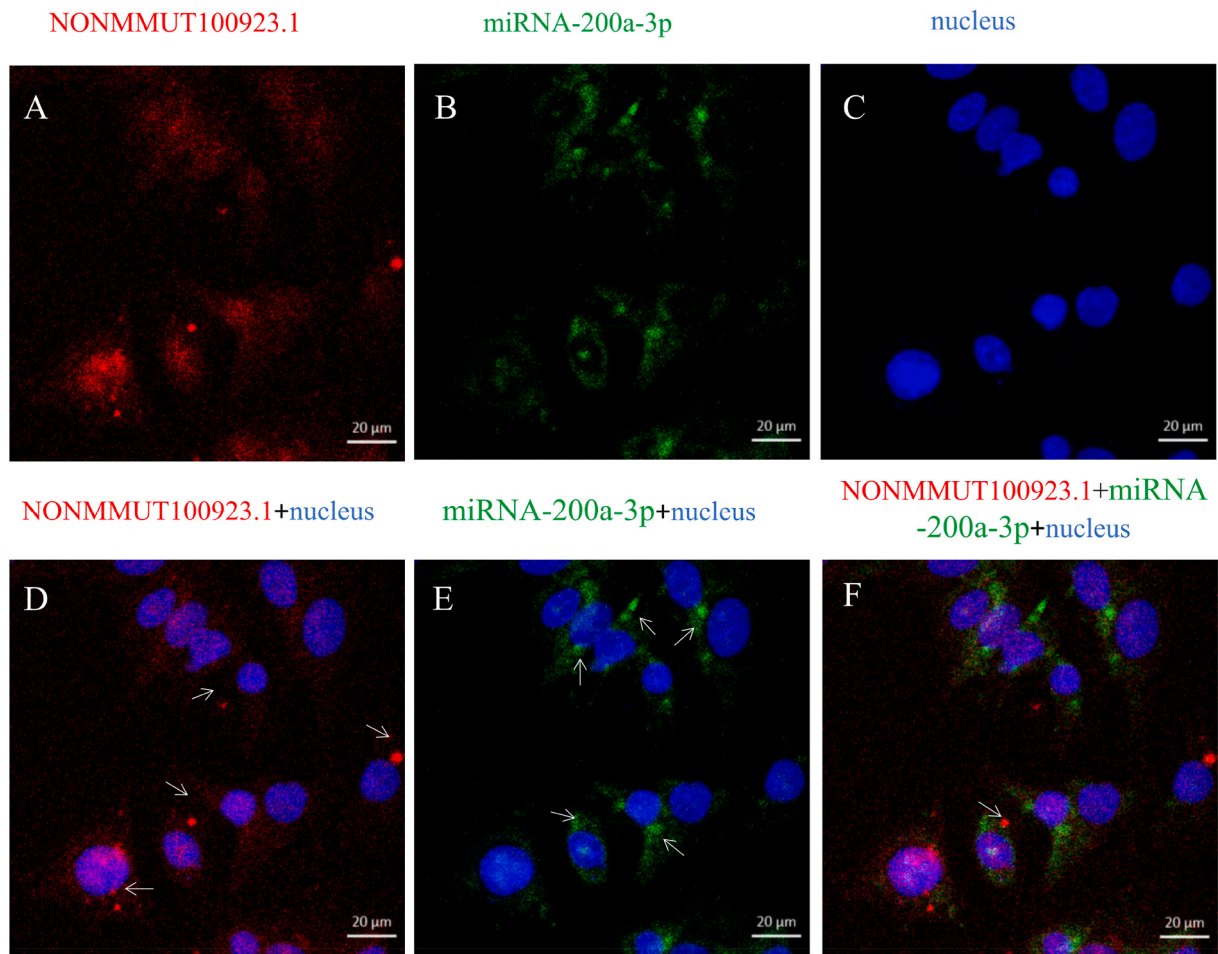


**Fig. 7.** The Fish assay analysis. The FISH assay was used to detect the subcellular location of NONMMUT100923.1 and miR-200a-3p in mouse MEPS epithelial cells in normal group at E16.5. (A)NONMMUT100923.1 (red); (B) miR-200a-3p (green); (C) the nucleus (blue); (D) The merging image of NONMMUT100923.1 (the white arrows) and nucleus; (E) The merging image of miR-200a-3p (the white arrows) and nucleus; (F) The merging image of NONMMUT100923.1, miR-200a-3p and nucleus (the white arrow indicate colocation of NONMMUT100923.1 and miR-200a-3p).

we performed RNA-seq analysis on mouse embryonic palatal shelves obtained from normal and model (cleft palate induced by retinoic acid) on E16.5. LncRNA-NONMMUT100923.1 was significantly upregulated in model group compared to normal group and this was further confirmed by RT-PCR assay. To the best of our knowledge, this is the first time that LncRNA-NONMMUT100923.1 was reported to be upregulated in this cleft palate model. This finding may expand the possibility of a new lncRNA regulatory pathway in the development of cleft palate and provides a new direction of gene targeted therapy for cleft palate.

MiRNA is a class of non-coding small RNA molecules with a length of about 22 nt and regulate of many disease [32,33], which are reported to be crucial for maxillofacial development [34]. miR-200a-3p belongs to the miR-200 family, whose biological significance and functional mechanisms in cleft palate are not clear. Many studies have reported that miR-200a-3p are involved in the tumorigenesis regulating cell proliferation and apoptosis [18,35]. It was also reported to be associated with various genes involved in the cleft lip by bioinformatic analysis, but the overexpression of miR-200a-3p did not seem to influence the proliferation of mouse embryonic lip mesenchymal cells [36]. In the current study, miR-200a-3p was significantly down-regulated in the model group with cleft palate, which contrasted with the expression of LncRNA-NONMMUT100923.1. On the other hand, complementary binding sites between LncRNA-NONMMUT100923.1 and miR-200a-3p was predicted and validated in our study. The sponging effects of LncRNA-NONMMUT100923.1 on miR-200a-3p was further demonstrated by colocalizing within the MEPS epithelial cells. Thus, the miR-200a-3p may be a key factor in the LncRNA-NONMMUT100923.1 regulatory pathway during cleft palate formation.

EMT is required for medial epithelial seam degeneration during palatal shelf fusion [37]. Desmosomes are pivotal anchoring structures and signaling pivots that regulate EMT via the induction of desmosome dissociation and disruption of cell-cell adhesive junctions [38]. *Cdsn* is a vital glycoprotein specifically found on desmosomes, which are in the medial edge epithelial cell layer [6,8,39]. *Cdsn* regulates cell-cell adhesion and intercellular junctions, which are essential for mammalian development. During the palate development at E14.5, the palatal shelves began to make contact and adhere. Then, the midline epithelial seam is formed, a process indicating the start of palatal fusion [40]. This process is accompanied by an increased number of desmosomes in the MEE at E14.5 [6].

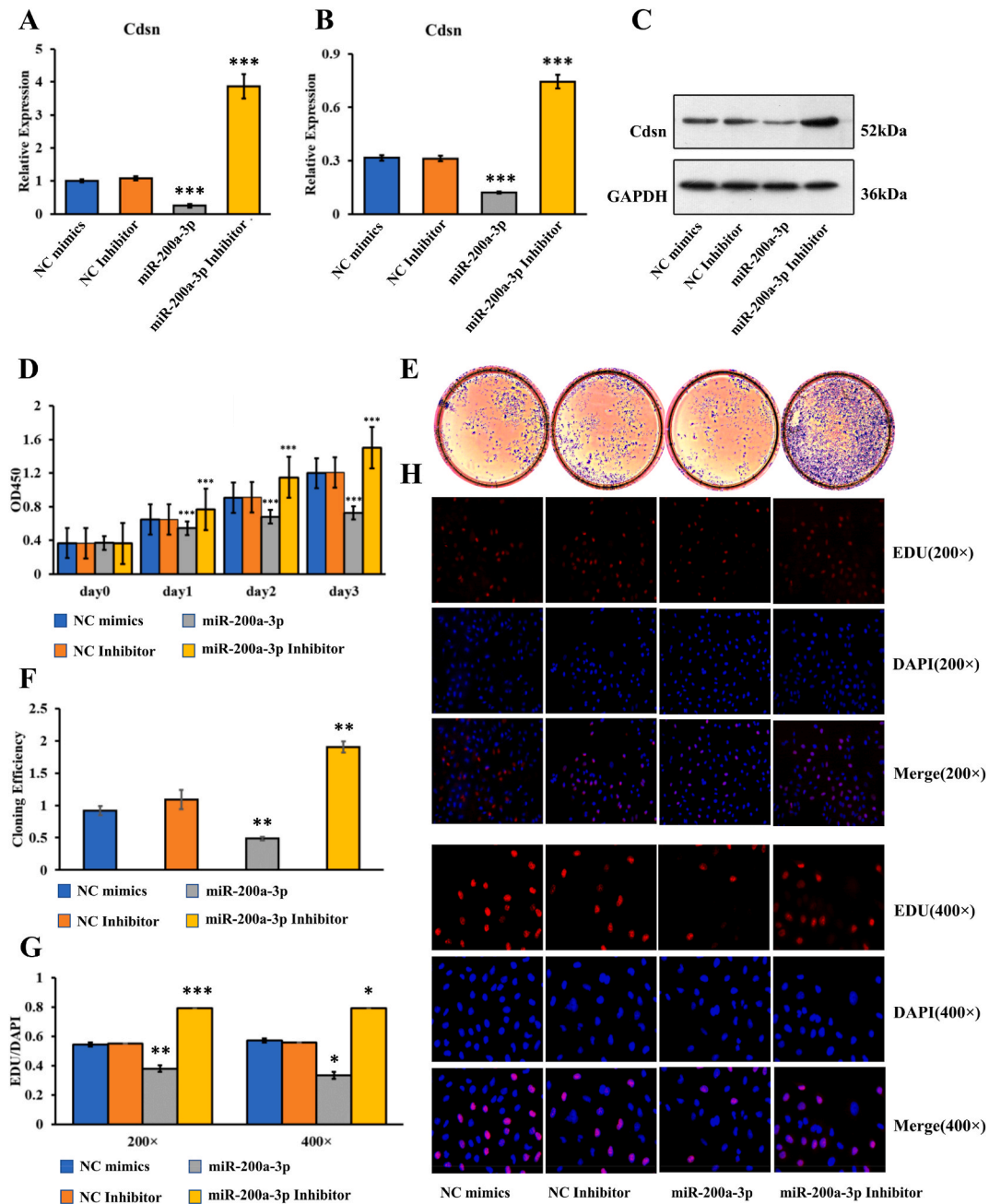


**Fig. 8.** Cell transfection analysis. The MEPS epithelial cells were transfected with NC mimics, inhibition, miR-200a-3p and miR-200a-3p inhibition group; (A) The RT-PCR assay were used to detect the gene expression level of *Cdsn* in transfected cells (\*\*\*)  $P < 0.001$ : miR-200a-3p vs. NC mimics and miR-200a-3p inhibitor vs. NC mimics); (B)The Western blot assay were used to detect the protein level expression of *Cdsn* in transfected cells (\*\*\*)  $P < 0.001$ : miR-200a-3p vs. NC mimics and miR-200a-3p inhibitor vs. NC mimics); (C) miR-200a-3p inhibitor positively upregulated the expression of *Cdsn* by Western blot (the original images of the Western blot was provided as supplemental f. 1); (D)The CCK-8 assay was performed to determine the proliferation of the transfected cells on day 0, day 1, day 2, day 3.(\*\*\*)  $P < 0.001$ : miR-200a-3p vs. NC mimics and miR-200a-3p inhibitor vs. NC mimics); (E) images of crystal violet-stained colonies; (F) The colony assay were used to determine the colony formation in the transfected cells (\*\*\*)  $P < 0.01$ : miR-200a-3p vs. NC mimics and miR-200a-3p inhibitor vs. NC mimics); (G) The Edu assay were used to determine the proliferation ability of the transfected cells. In 200x, \*\*\*)  $P < 0.01$ : miR-200a-3p vs. NC mimics; (\*\*\*)  $P < 0.001$ : miR-200a-3p inhibitor vs. NC mimics. In 400x, \*)  $P < 0.05$ : miR-200a-3p vs. NC mimics and miR-200a-3p inhibitor vs. NC mimics); (H) Images of Edu assay in 200x and 400x. Data are presented as mean  $\pm$  SD from 3 independent samples.

After EMT of the MEE, the desmosome dissociates. In this study, *Cdsn* was significantly upregulated in palatal shelves in the model group at E16.5, which indicates that the desmosome was consistently expressed on MEE epithelial cells. This may lead to the persistence of cell–cell adhesive junctions that prevent EMT from E14.5 until E16.5 [41]. This inappropriate adhesion of MEE cells may result in the dysfunction of the EMT and separation of the embryonic palatal shelves, which is consistent with CP formation in the embryos at E16.5. Furthermore, *Cdsn* was demonstrated to be a target gene of miR-200a-3p and the inhibition of miR-200a-3p can significantly upregulate its expression levels in MEPS epithelial cells accompanied with increased level of MEPS epithelial cells proliferation. On the other hand, EMT is accompanied with the loss of epithelial cell junction proteins and gain of mesenchymal markers. The significant upregulation of epithelial marker: *Cldn10* [42], *Itgb4* [43], *Pax9* [44], and *Itga3* [45] may disturb the EMT process by promoting the MEPS epithelial cells proliferation, which may also be involve in this ceRNA regulatory network. Taking together, these may indicate that the lncRNA-NONMMUT100923.1 could regulate *Cdsn* expression by competitively binding to endogenous miR-200a-3p. This ceRNA regulatory network may inhibit mouse embryonic palatal shelf adhesion and fusion by preventing the disintegration of the desmosome junction or affecting the epithelial cell proliferation in the MEE.

## 5. Conclusion

We showed that lncRNA-NONMMUT100923.1 may serve as ceRNA to increase *Cdsn* expression by sponging miR-200a-3p. This may regulate mouse embryonic palatal shelf adhesion by maintaining the epithelial desmosome junction during palatogenesis. lncRNA-NONMMUT100923.1 may act as a ceRNA to competitively bind to miR-200a-3p and upregulate *Cdsn* expression, thereby enhancing the stability and elasticity of the desmosome junction in MEE cells. The desmosome junction may serve as an anchorage point for MEE epithelial cells to inhibit the proliferation, differentiation, migration, and EMT of MEE epithelial cells, which may lead to CP formation. Our study suggests strategies for therapeutic intervention to prevent or treat CP.

### 5.1. Limitations of the study

However, this study had some limitations. First, the samples size for sequencing (model:  $n = 3$  vs. normal:  $n = 3$ ) was relatively small. Second, the direct effects of lncRNA-NONMMUT100923.1/miR-200a-3p/*Cdsn* axis on EMT needs further investigation. For example, whether this axis can affect the expression levels of several key regulators of EMT, like *Cldn10*, *Itgb4*, *Pax9*, and *Itga3* in MEPS epithelial cells or in the cleft palate tissues or not. Also, the expression patterns of this axis during the formation of CP should be further investigated. Finally, localizing the expression of desmosomes by immunohistochemical analysis in the MEE cell on E16.5 normal and model groups is necessary in the future.

### Ethics approval and consent to participate

This study was performed in accordance with and approved by the guidelines of the Animal Experiment Center of Shantou University Medical College (SUMC2019-297).

### Consent for publication

Not applicable.

### Author contribution statement

Ming Zhang, Jiayan Zhou: Conceived and designed the experiments; Performed the experiments; Analyzed and interpreted the data; Contributed reagents, materials, analysis tools or data; Wrote the paper.

Yingwen Ji: Conceived and designed the experiments; Performed the experiments; Analyzed and interpreted the data.

Shuyou Shen, Mingjun Zhang, Yan Liang: Conceived and designed the experiments; Analyzed and interpreted the data.

### Funding statement

Shenyou Shu was supported by Natural Science Foundation of Guangdong Province {2019A1515010346}.

Yan Liang was supported by Youth and Middle-aged Scientific and Technological Innovation Leading Talents Program of the Corps {190917085269837}.

### Data availability statement

Data associated with this study has been deposited at <https://data.mendeley.com/datasets/rrh24wdc54/draft?a=9da79b3b-5036-4c49-abb2-ebf48954a00d>.

### Declaration of competing interest

The authors declare that they have no known competing financial interests or personal relationships that could have appeared to

influence the work reported in this paper.

## Acknowledgements

We would like to thank Editage ([www.editage.cn](http://www.editage.cn)) for English language editing.

## Abbreviations

lncRNA: Long non-coding RNA; Cdsn: Corneodesmosin; CP: Cleft palate; CeRNA: Competing endogenous RNA; MEPS: Mouse embryonic palatal shelf; MEE: Medial edge epithelium; MET: Epithelial-mesenchymal transition; MREs: miRNA response elements; RT-PCR: Reverse transcription-polymerase chain reaction; WB: Western blotting; FISH: Fluorescence in situ hybridization; CCK-8: Cell counting kit-8; EdU: 5-Ethynyl-2'-deoxyuridine.

## Appendix. ASupplementary data

Supplementary data related to this article can be found at <https://doi.org/10.1016/j.heliyon.2023.e16329>.

## References

- [1] A. Gritli-Linde, Molecular control of secondary palate development, *Dev. Biol.* 301 (2007) 309–326, <https://doi.org/10.1016/j.ydbio.2006.07.042>.
- [2] A. Nawshad, Palatal seam disintegration: to die or not to die? that is no longer the question, *Dev. Dynam.* 237 (2008) 2643–2656, <https://doi.org/10.1002/dvdy.21599>.
- [3] C.F. Shuler, Y. Guo, A. Majumder, R.Y. Luo, Molecular and morphologic changes during the epithelial-mesenchymal transformation of palatal shelf medial edge epithelium in vitro, *Int. J. Dev. Biol.* 35 (1991) 463–472.
- [4] M. Ozawa, W. Kobayashi, Cadherin cytoplasmic domains inhibit the cell surface localization of endogenous E-cadherin, blocking desmosome and tight junction formation and inducing cell dissociation, *PLoS One* 9 (2014), e105313, <https://doi.org/10.1371/journal.pone.0105313>.
- [5] M.W. Ferguson, Palate development: mechanisms and malformations, *Ir. J. Med. Sci.* 156 (1987) 309–315, <https://doi.org/10.1007/BF02951261>.
- [6] M. Mogass, P. Bringas Jr., C.F. Shuler, Characterization of desmosomal component expression during palatogenesis, *Int. J. Dev. Biol.* 44 (2000) 317–322.
- [7] A. Nakajima, A.O.D. Gulka, J.I. Hanai, TGF-Beta signaling and the epithelial-mesenchymal transition during palatal fusion, *Int. J. Mol. Sci.* 19 (2018), <https://doi.org/10.3390/ijms19113638>.
- [8] E.A. Leclerc, A. Hucheng, N.R. Mattiuzzo, D. Metzger, P. Chambon, N.B. Ghyselinck, G. Serre, N. Jonca, M. Guerrin, Corneodesmosin gene ablation induces lethal skin-barrier disruption and hair-follicle degeneration related to desmosome dysfunction, *J. Cell Sci.* 122 (2009) 2699–2709, <https://doi.org/10.1242/jcs.050302>.
- [9] M.J. Dixon, M.L. Marazita, T.H. Beaty, J.C. Murray, Cleft lip and palate: understanding genetic and environmental influences, *Nat. Rev. Genet.* 12 (2011) 167–178, <https://doi.org/10.1038/nrg2933>.
- [10] F. Rahimov, A. Jugessur, J.C. Murray, Genetics of nonsyndromic orofacial clefts, *Cleft Palate Craniofac J* 49 (2012) 73–91, <https://doi.org/10.1597/10-178>.
- [11] M.A. Shkoukani, M. Chen, A. Vong, Cleft lip - a comprehensive review, *Front Pediatr* 1 (2013) 53, <https://doi.org/10.3389/fped.2013.00053>.
- [12] G. Nasreddine, J. El Hajj, M. Ghassibe-Sabbagh, Orofacial clefts embryology, classification, epidemiology, and genetics, *Mutat. Res. Rev. Mutat. Res.* 787 (2021), 108373, <https://doi.org/10.1016/j.mrrev.2021.108373>.
- [13] S.E. Watkins, R.E. Meyer, R.P. Strauss, A.S. Aylsworth, Classification, epidemiology, and genetics of orofacial clefts, *Clin. Plast. Surg.* 41 (2014) 149–163, <https://doi.org/10.1016/j.cps.2013.12.003>.
- [14] L. Salmena, L. Poliseno, Y. Tay, L. Kats, P.P. Pandolfi, A ceRNA hypothesis: the Rosetta Stone of a hidden RNA language? *Cell* 146 (2011) 353–358, <https://doi.org/10.1016/j.cell.2011.07.014>.
- [15] X. Liu, H. Liu, Y. Wu, Z. He, L. Shen, H. Zhang, Z. Wan, Y. Chen, H. Yue, T. Zhang, S. Gao, Z. Yu, The role of lncRNA Meg3 in the proliferation of all-trans retinoic acid-treated mouse embryonic palate mesenchymal cells involves the Smad pathway, *Reprod. Toxicol.* 104 (2021) 1–7, <https://doi.org/10.1016/j.reprotox.2021.06.011>.
- [16] X. Liu, Y. Zhang, L. Shen, Z. He, Y. Chen, N. Li, X. Zhang, T. Zhang, S. Gao, H. Yue, Z. Li, Z. Yu, LncRNA Meg3-mediated regulation of the Smad pathway in atRA-induced cleft palate, *Toxicol. Lett.* 341 (2021) 51–58, <https://doi.org/10.1016/j.toxlet.2021.01.017>.
- [17] W. Gong, Y. Cao, Y. Wang, L. Yang, W. Su, F. Qiu, S. Datta, B. Rao, J. Xian, M. Lin, Y. Feng, X. Zhang, Y. Zhou, X. Gao, J. Lu, Upregulation of lncRNA FEZF-AS1 is associated with advanced clinical stages and family history of cancer in patients with NSCLC, *Pathol. Res. Pract.* 214 (2018) 857–861, <https://doi.org/10.1016/j.prp.2018.04.014>.
- [18] W. Lv, Y. Jia, J. Wang, Y. Duan, X. Wang, T. Liu, S. Hao, L. Liu, Long non-coding RNA SNHG10 upregulates BIN1 to suppress the tumorigenesis and epithelial-mesenchymal transition of epithelial ovarian cancer via sponging miR-200a-3p, *Cell Death Dis.* 8 (2022) 60, <https://doi.org/10.1038/s41420-022-00825-9>.
- [19] M.X. Sun, H.Y. An, Y.B. Sun, Y.B. Sun, B. Bai, LncRNA EBLN3P attributes methotrexate resistance in osteosarcoma cells through miR-200a-3p/O-GlcNAc transferase pathway, *J. Orthop. Surg. Res.* 17 (2022) 557, <https://doi.org/10.1186/s13018-022-03449-y>.
- [20] F. Qin, Z. Shen, L. Peng, R. Wu, X. Hu, G. Zhang, S. Tang, Metabolic characterization of all-trans-retinoic acid (ATRA)-induced craniofacial development of murine embryos using in vivo proton magnetic resonance spectroscopy, *PLoS One* 9 (2014), e96010, <https://doi.org/10.1371/journal.pone.0096010>.
- [21] S. Anders, W. Huber, Differential expression of RNA-Seq data at the gene level – the DESeq package, *embl* (2021).
- [22] NS, Practical Plastic Surgery for Non Surgeons, Hanley&Belfus, Inc, Philadelphia, 2001, pp. 235–243.
- [23] T.H. Beaty, J.C. Murray, M.L. Marazita, R.G. Munger, I. Ruczinski, J.B. Hetmanski, K.Y. Liang, T. Wu, T. Murray, M.D. Fallin, R.A. Redett, G. Raymond, H. Schwender, S.C. Jin, M.E. Cooper, M. Dunnwald, M.A. Mansilla, E. Leslie, S. Bullard, A.C. Lidral, L.M. Moreno, R. Menezes, A.R. Vieira, A. Petrin, A.J. Wilcox, R.T. Lie, E.W. Jabs, Y.H. Wu-Chou, P.K. Chen, H. Wang, X. Ye, S. Huang, V. Yeow, S.S. Chong, S.H. Jee, B. Shi, K. Christensen, M. Melbye, K.F. Doheny, E. W. Pugh, H. Ling, E.E. Castilla, A.E. Czeizel, L. Ma, L.L. Field, L. Brody, F. Pangilinan, J.L. Mills, A.M. Molloy, P.N. Kirke, J.M. Scott, M. Arcos-Burgos, A.F. Scott, A genome-wide association study of cleft lip with and without cleft palate identifies risk variants near MAFB and ABCA4, *Nat. Genet.* 42 (2010) 525–529, <https://doi.org/10.1038/ng.580>.
- [24] G.L. Wehby, C.H. Cassell, The impact of orofacial clefts on quality of life and healthcare use and costs, *Oral Dis.* 16 (2010) 3–10, <https://doi.org/10.1111/j.1601-0825.2009.01588.x>.
- [25] A. Heliövaara, A. Kuseler, P. Skaare, H. Bellardie, K. Molsted, A. Karsten, A. Marcusson, S. Rizell, E. Brinck, P. Saele, M.N. Chalien, J. Mooney, P. Eyres, W. Shaw, G. Semb, Scandicleft randomized trials of primary surgery for unilateral cleft lip and palate: comparison of dental arch relationships and dental indices at 5, 8, and 10 years, *Eur. J. Orthod.* 44 (2022) 258–267, <https://doi.org/10.1093/ejo/cjab055>.
- [26] J. Lilja, Cleft lip and palate surgery, *Scand. J. Surg.* 92 (2003) 269–273, <https://doi.org/10.1177/145749690309200406>.

- [27] T. Ali, P. Grote, Beyond the RNA-dependent function of lncRNA genes, *Elife* 9 (2020), <https://doi.org/10.7554/eLife.60583>.
- [28] Y. Pan, C. Li, J. Chen, K. Zhang, X. Chu, R. Wang, L. Chen, The emerging roles of long noncoding RNA ROR (lincRNA-ROR) and its possible mechanisms in human cancers, *Cell. Physiol. Biochem.* 40 (2016) 219–229, <https://doi.org/10.1159/000452539>.
- [29] D. Vidovic, T.T. Huynh, P. Konda, C. Dean, B.M. Cruickshank, M. Sultan, K.M. Coyle, S. Gujar, P. Marcato, ALDH1A3-regulated long non-coding RNA NRAD1 is a potential novel target for triple-negative breast tumors and cancer stem cells, *Cell Death Differ.* 27 (2020) 363–378, <https://doi.org/10.1038/s41418-019-0362-1>.
- [30] X. Wang, S. Guo, X. Zhou, Y. Wang, T. Zhang, R. Chen, Exploring the molecular mechanism of lncRNA-miRNA-mRNA networks in non-syndromic cleft lip with or without cleft palate, *Int. J. Gen. Med.* 14 (2021) 9931–9943, <https://doi.org/10.2147/IJGM.S339504>.
- [31] L. Gao, Y. Liu, Y. Wen, W. Wu, lncRNA H19-mediated mouse cleft palate induced by all-trans retinoic acid, *Hum. Exp. Toxicol.* 36 (2017) 395–401, <https://doi.org/10.1177/0960327116651121>.
- [32] H. Matsuyama, H.I. Suzuki, Systems and synthetic microRNA biology: from biogenesis to disease pathogenesis, *Int. J. Mol. Sci.* 21 (2019), <https://doi.org/10.3390/ijms21010132>.
- [33] C.J. Stavast, S.J. Erkeland, The non-canonical aspects of MicroRNAs: many roads to gene regulation, *Cells* 8 (2019), <https://doi.org/10.3390/cells8111465>.
- [34] J.O. Shin, J.M. Lee, K.W. Cho, S. Kwak, H.J. Kwon, M.J. Lee, S.W. Cho, K.S. Kim, H.S. Jung, MiR-200b is involved in Tgf-beta signaling to regulate mammalian palate development, *Histochem. Cell Biol.* 137 (2012) 67–78, <https://doi.org/10.1007/s00418-011-0876-1>.
- [35] H. Chen, L. Gu, M. Zhang, H. Chen, H. Liao, X. Cao, L. Yu, J. Zhang, Interaction of miR-200a-3p with YAP regulates cell proliferation and metastasis differentially in HPV-positive and HPV-negative cervical cancer cells, *BMC Cancer* 22 (2022) 1039, <https://doi.org/10.1186/s12885-022-10118-0>.
- [36] H. Yoshioka, S.S. Ramakrishnan, A. Suzuki, J. Iwata, Phenytoin inhibits cell proliferation through microRNA-196a-5p in mouse lip mesenchymal cells, *Int. J. Mol. Sci.* 22 (2021), <https://doi.org/10.3390/ijms22041746>.
- [37] R. Cuervo, L. Covarrubias, Death is the major fate of medial edge epithelial cells and the cause of basal lamina degradation during palatogenesis, *Development* 131 (2004) 15–24, <https://doi.org/10.1242/dev.00907>.
- [38] P. Savagner, K.M. Yamada, J.P. Thiery, The zinc-finger protein slug causes desmosome dissociation, an initial and necessary step for growth factor-induced epithelial-mesenchymal transition, *J. Cell Biol.* 137 (1997) 1403–1419, <https://doi.org/10.1083/jcb.137.6.1403>.
- [39] N. Siva Subramaniam, E. Morgan, S. Bottomley, S. Tay, K. Gregg, C.Y. Lee, J. Wetherall, D. Groth, Predictive mutational bioinformatic analysis of variation in the skin and wool associated corneodesmosin (CDSN) gene in sheep, *Anim. Sci. J.* 83 (2012) 386–393, <https://doi.org/10.1111/j.1740-0929.2011.00975.x>.
- [40] J.O. Bush, R. Jiang, Palatogenesis: Morphogenetic and Molecular Mechanisms of Secondary Palate Development, *Development*, 2012, pp. 231–243, <https://doi.org/10.1242/dev.067082>.
- [41] V. Kaartinen, X.-M. Cui, N. Heisterkamp, J. Groffen, C.F. Shuler, Transforming growth factor- $\beta$ 3 regulates transdifferentiation of medial edge epithelium during palatal fusion and associated degradation of the basement membrane, *Dev. Dynam.* 209 (1997) 255–260, [https://doi.org/10.1002/\(sici\)1097-0177\(199707\)209:3](https://doi.org/10.1002/(sici)1097-0177(199707)209:3).
- [42] I. Hashimoto, T. Oshima, Claudins and gastric cancer: an overview, *Cancers* 14 (2022), <https://doi.org/10.3390/cancers14020290>.
- [43] Z. Liu, T. Sun, C. Piao, Z. Zhang, C. Kong, METTL14-mediated N(6)-methyladenosine modification of ITGB4 mRNA inhibits metastasis of clear cell renal cell carcinoma, *Cell Commun. Signal.* 20 (2022) 36, <https://doi.org/10.1186/s12964-022-00831-5>.
- [44] M. Shi, S. Ren, H. Chen, J. Li, C. Huang, Y. Li, Y. Han, Y. Li, Z. Sun, X. Chen, Z. Xiong, Alcohol drinking inhibits NOTCH-PAX9 signaling in esophageal squamous epithelial cells, *J. Pathol.* 253 (2021) 384–395, <https://doi.org/10.1002/path.5602>.
- [45] H. Zhang, X. Cui, A. Cao, X. Li, L. Li, ITGA3 interacts with VASP to regulate stemness and epithelial-mesenchymal transition of breast cancer cells, *Gene* 734 (2020), 144396, <https://doi.org/10.1016/j.gene.2020.144396>.